Assessment of hydrogen flame visibility – Phase 2

Project number: RP1.4-10

December 2024

Project number: RP1.4-10

Assessment of hydrogen flame visibility

Authors:

Yilong Yin, Douglas Proud, Paul Medwell

Project team:

Scott Sharbanee (Enscope)

Rebecca Searcy (Energy Safe Victoria)

Ben Greeneklee (Electrolux)

Robert Davis (Australian Gas Infrastructure Group)

Douglas Proud (The University of Adelaide / Future Fuels CRC)

Neil Smith (The University of Adelaide)

Peter Ashman (The University of Adelaide)

Paul Medwell (The University of Adelaide)

Australian Government

Department of Industry, Science and Resources

Cooperative Research Centres Program

This work is funded by the Future Fuels CRC, supported through the Australian Government's Cooperative Research Centres Program. We gratefully acknowledge the cash and in-kind support from all our research, government and industry participants.

IMPORTANT DISCLAIMER

Future Fuels CRC advises that the information contained in this report comprises statements based on research. Future Fuels CRC makes no warranty, express or implied, for the accuracy, completeness or usefulness of such information or represents that its use would not infringe privately owned rights, including any parties intellectual property rights. To the extent permitted by law, Future Fuels CRC (including its employees and Participants) excludes all liability to any person for any consequences, including but not limited to all losses, damages, costs, expenses and any other compensation, arising directly or indirectly from using this report (in part or in whole) and any information or material contained in it.

PROJECT INFORMATION	
Project number	RP1.4-10
Project title	Assessment of hydrogen flame visibility
Research Program	RP1 – Future Fuel Technologies, Systems and Markets
Milestone Report Number	2
Description	Summary of experimental findings on impacts affecting the colour and visibility of hydrogen flames.
Research Provider	The University of Adelaide
Project Leader and Team	Paul Medwell, Douglas Proud, Neil Smith, Peter Ashman (The University of Adelaide)
Industry Proponent and Advisor Team	Scott Sharbanee (Enscope) Rebecca Searcy (Energy Safe Victoria) Ben Greeneklee (Electrolux) Robert Davis (AGIG)
Related Commonwealth Schedule	RP1.4.2: Solutions for new/modified household appliances and meters to allow for a broader range of fuel compositions delivered. RP1.4.4: Provision of recommendations, based on research into modification needs for appliances and equipment, for updates of appliance standards.
Project start/completion date	01-DEC-2023 / 20-DEC-2024
IP Access	**Restricted** – available to participants only
Approved by	
Date of approval	

Table of Contents

Project Information 4
Summary of Report 6
1 Introduction 7
2 Background 8
2.1 Electromagnetic radiation emissions from flames 8
2.2 Hydrogen flame colours 10
2.3 Atmospheric sodium distribution and detection 11
3 Experimental Setup 14
3.1 Burner designs 14
3.2 Diagnostic techniques 14
3.3 Variables 15
4 Results and Discussion 17
4.1 Simple open jet flames 17
4.2 Cooktop flames 22
4.3 Photographs under different lighting conditions 26
4.4 Correlation between spectrometry and photographs 27
4.5 Spectrometry data at different locations 28
4.6 Anecdotal observations 29
5 Conclusions 32
6 Implications and Recommendations for Industry 33
7 References 34

Summary of Report

This report provides a summary of experimental findings into the colour and visibility of hydrogen flames. The primary focus is on domestic appliances (classified as “Type A” appliances in Australia) where flame visibility can be a significant safety control measure, but the findings have implications for other scenarios.

The project aims to isolate and quantify the factors that may influence hydrogen flame visibility, and to determine if flame visibility can be relied upon as an indicator of flame presence in a similar way that natural gas flames are expected to be visible in a domestic setting. Based on previous work, both in the literature and from the experience of the project team, a variety of colours have been used to describe hydrogen flames. A widely reported finding is that hydrogen flames can be difficult to see, thus presenting a hazard whereby individuals could inadvertently come in contact with a naked flame. In the context of hydrogen amongst the community in a domestic setting, it is critical to understand the factors that affect the colour and visibility of hydrogen flames, which are distinctly different to natural gas.

In the first phase of this project, the focus was on understanding the fundamental factors that influence hydrogen flame visibility and colour. Through a series of controlled lab-based experiments, it was identified that the most dominant colour of hydrogen flames is orange. This colour was attributed to sodium in the atmosphere. Hydrogen flames can also have a red and/or blue appearance; however, these colours are much weaker than the orange. When the orange colour is suppressed, the flames become nearly invisible in a typical well-lit kitchen environment.

In the second phase of this project, the correlation between the influencing factors of sodium in the ambient air and the visibility of hydrogen flames have been compared with natural gas flames on a domestic appliance under real-world conditions. It is found that wind direction from over the ocean appears to be the primary factor for higher orange colouration and wind direction from over terrestrial (land) areas has distinctly lower colourisation of the flame. There is much less correlation with other environmental conditions, such as temperature and humidity.

Because of the strong dependence on wind direction, the extent of orange flame colouration varies on a daily basis. In all scenarios tested as part of this project, no real-world conditions were able to be achieved that reduced the orange colour to the point it could not be distinguished. However, anecdotal observations of a hydrogen flame in a clean room reinforced that, despite the inherent red/blue colours of hydrogen flames, these flames can be nearly invisible, even in a darkened room. This reinforces that adventitious sodium in practical settings is therefore an important control measure for ensuring visibility. The reliance on naturally occurring sodium to ensure flame visibility is unreliable, because it strongly depends on factors beyond the control of appliance designers or technical regulators. Alternative means of indicating the presence of a hydrogen flame should be considered.

Overall, even in the most amenable conditions, cooktop hydrogen flames are on average much less luminous than natural gas flames — although some intermittent orange flamelets may instantaneously be of a similar intensity.

1 Introduction

Application of open flames in proximity to humans relies on flames being visible under all relevant conditions, as a safety measure to prevent injury. Identification of natural gas (NG) is widely understood by the broad community, providing key safety features that can be relied upon to mitigate the risk of unintended releases escalating to major incidents. When NG burns it has a distinctive yellow and/or blue colouration, giving a visual indication of the presence of a flame. In assessing the suitability of hydrogen as a replacement for NG in domestic settings, it is important to ensure that key safety features can be relied upon in an equivalent and familiar manner to NG. In contrast to NG, hydrogen does not exhibit a consistent and naturally distinctive and familiar flame colour when it burns; hence, visible identification of hydrogen in a domestic consumer setting may not be a feature that can be relied upon in these applications.

The issue of flame visibility, specifically the colour of hydrogen flames, has been mentioned in previous Future Fuels CRC projects (refer Section 2.1). The general consensus is that hydrogen flames for some typical domestic appliances have some visible emissions, and the source of the light can usually be attributed to known processes under laboratory conditions. However, the visibility in uncontrolled real-world settings is also believed to be highly variable to local conditions. Therefore, any assumptions about flame visibility may be based on incomplete or ill-conditioned evidence. The poorly understood nature of hydrogen flame visibility in a range of conditions likely to be encountered by residential customers will be important for consumer acceptance and potentially represents a critical safety barrier. This project aims to provide an improved understanding of the factors which affect hydrogen flame visibility and how this translates to real-world conditions. In the context of this project, the focus is on unblended hydrogen, without the presence of hydrocarbons in the fuel stream.

In the first phase of this project, the visibility of hydrogen flames has been investigated on a jet burner under laboratory conditions through a combination of photography and spectroscopy. It has been identified that hydrogen flames appear orange due to the presence of sodium in ambient room air, which can have a significant impact on the visible light emitted from the flame. The key factors which influence the flame visibility have been evaluated and reported in the Phase 1 report. The source of air was the dominant factor, with other effects including flame conditions (premixed vs non-premixed), coflow conditions, and fuel velocity. Based on the understanding and findings from Phase 1, there is a need to investigate the hydrogen flame visibility and its influencing factors under real-world conditions.

The second phase of the project seeks to identify limiting conditions which influence hydrogen flame visibility under real-world conditions, and to what extent the environmental aspects affect the visibility through spectrometry and photography. The intended outcome of the project will identify and summarise which variables impact flame colour, and which combination of variables leads to the best outcome for flame colour for aesthetic purposes or where a visible flame could be considered a safety control measure.

2 Background

2.1 ELECTROMAGNETIC RADIATION EMISSIONS FROM FLAMES

Flames emit radiation across the electromagnetic spectrum, ranging from infrared through to ultraviolet [1,2,3]. Broadly, the emissions can be attributed to two processes: incandescence and luminescence.

Incandescence is the broadband emission of electromagnetic radiation from a body due to its temperature. In the context of flames, this phenomenon occurs when solid particles, primarily soot, are heated. The spectrum of light emitted by these incandescent particles is continuous, spanning a range of wavelengths. The peak wavelength and overall distribution are determined by the temperature of the emitting body, respectively described by Wien's Law and Planck's Law. As the temperature increases, the peak of the emission spectrum shifts from longer wavelengths (red) towards shorter wavelengths (blue).

Luminescence refers to light that is emitted from excited chemical species that subsequently return to their ground state [1]. When these energised species return to their ground state, the difference in the energy states is emitted as light of a wavelength specific to that difference. In a combustion system, this is typically via chemiluminescence, and whilst the emission spectra are often in the visible range, many also lie in the infrared or ultraviolet regions [3]. Examples with a narrow emission band include; CH* in the blue range [4], and OH* in the ultraviolet range [5]. Other species emit light through thermal excitation at a series of discrete wavelengths but over a broad range, for example, C_2* in the green range (known as the Swan bands) [6], CO_2* in the blue region of the visible spectrum [7], and thermally excited H_2O* water in the red / infra-red region [2,8].

By way of illustrative example, consider the case of a natural gas flame on a Bunsen burner in each of the two distinct modes of operation. When the flame is aerated (i.e. partially premixed) the flame has low levels of soot, and the colour is dominated by luminescence from CH* radicals that are formed in the reaction zone, giving the characteristic blue colouration. When operated as a non-premixed flame, soot is produced, leading to the distinctive yellow colour from the incandescence of the soot particles. The blue colouration from CH* luminescence persists in the sooting flame, but the intensity from the incandescence tends to dominate and gives the yellow colouration. Worth noting is that the colour from incandescence does change as a function of temperature — red/orange colour if cooler, or white/blue if hotter — however, no flame achieves a temperature to achieve blue colour due to incandescence. A further feature of the blue emissions from CH* is that the light is at a series of discrete wavelengths, owing to the relaxation of energy between quantum levels in the CH radical. In contrast, the colouration due to incandescence is a continuum, spanning a wide range of wavelengths.

Figure 1 shows the measured spectra from a self-aspirated burner, comparing the intensity and spectral location of the light emissions when operating on natural gas and hydrogen. The corresponding table reports origin for the dominant wavelengths. The relative strength of the sodium (Na) emission at 589 nm is much stronger in these measurements than those reported elsewhere [9]. The source of sodium is discussed throughout this report.

When interpreting spectral data, it is important to distinguish the differences in how a spectrometer detects light compared with the human eye. Because the spectrometer separates light into specific wavelengths, it may appear to have a high intensity on the graph (e.g. the sodium peak at 589 nm). In comparison, light emitted over a broad range of wavelengths may not appear with high intensity on a spectrum but the integrated light over a spectral band (e.g. blue) may appear bright to a human. For example, in the natural gas spectrum shown in Figure 1, the highest intensity is the sodium line at 589 nm, but this has a very narrow bandwidth. The broad emissions, especially over the blue range (430–500 nm), tend to dominate the visual appearance of the flame. In other words, the area under the curve can be more dominant than any relatively high but narrow peak. Hence, even though this natural gas flames features a strong emission peak from sodium, it appears the common blue colour because the light emitted over the broader spectral range dominates the narrow-band sodium emission.

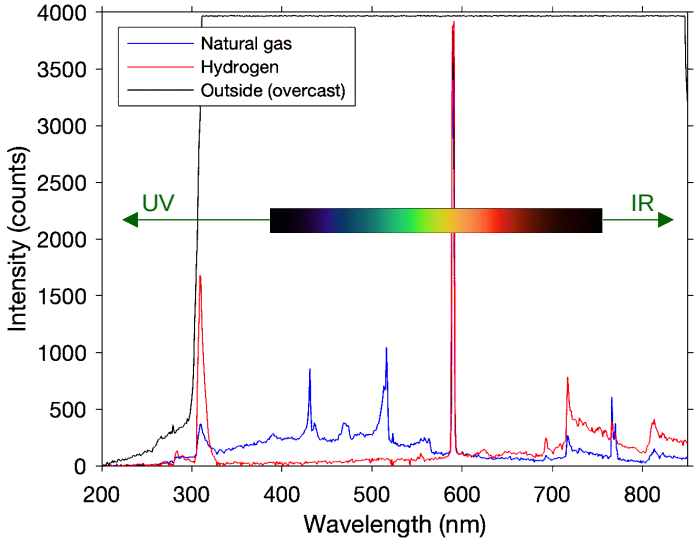

Approx. λ (nm)	Origin
310 (and 285)	OH*
430	CH*
515	C_2 Swan bands
589	Na
Visible continuum (400-700)	Soot and/or CO_2*
IR continuum (>700)	H_2O* (with some CO_2* peaks)

Figure 1: ***Emissions spectra of partially-premixed natural gas and non-premixed hydrogen flames in a commercial AN venturi burner, both supplied at 35 kW of fuel gas. The spectral emission profile taken outside on an overcast day is presented for comparison in the UV range. All data was collected with the same integration time on the spectrometer. Figure reproduced from Future Fuels CRC RP1.4-03 Final Report, overlaid with an indicative visible spectrum.***

The key features identified in Figure 1 can be attributed to the well-established spectra from atomic [10], molecular [11], and radical sources [12]. However, the relative intensity due to each contribution is dependent on a variety of factors, including:

- flame temperature
- mixing characteristics
- burner geometry and materials
- local environment
- lighting / background

In addition to these factors, the duration of operation is also known to have an influence on the flame colour: "*The flame starts less luminous but as it warms up and interacts with the atmosphere it becomes orange*" [13].

Flame visibility has been assessed in some previous Future Fuels CRC projects, including:

(a) RP1.10-04 (Effect of dopants on hydrogen flames for improved safety and performance). This project investigated the potential of doping hydrogen flames in a domestic setting with a hydrocarbon fuel additive to simultaneously achieve increased visibility, odourisation and improved radiative heat transfer. Toluene was identified as a potential candidate dopant, with at least 0.5 mol% needed to be added to hydrogen to achieve similar performance to NG, corresponding to 18.8% on a mass basis. Hence, whilst there may be some bespoke applications that would benefit from toluene addition, it is unlikely that toluene addition is a "catch all" solution. The report did, however, provide a variety of measurements comparing NG and hydrogen flames across a range of operating conditions, demonstrating the effects of sodium.

(b) RP1.4-03 (De-risking H_2 Adaptation to Industrial Processes). This project investigated methods to increase radiative heat transfer from industry-relevant burners, through addition of toluene. Although the focus was on heat transfer, the visible appearance of the flames was also inherently captured and was expanded in subsequent journal articles [14,15]. It was also identified that the relative visual brightness of

NG and hydrogen flames is affected by burner geometry. Appendix A of the Final Report also presented sample spectra for different flame conditions.

(c) RP1.4-05 (Performance of Type A appliances with blends of hydrogen and natural gas) and RP1.4-08 (Detailed assessment of Type B appliances with blends of hydrogen and natural gas and 100% hydrogen). Both these projects have assessed the development and testing of 100% hydrogen burners. Although not the primary objective of the work, flame appearance was clearly observed through the experiments. Bright orange flames were reported. Specific light emissions measurements were not collected, but anecdotal evidence is supportive of sodium colouration in these various flames.

2.2 HYDROGEN FLAME COLOURS

As identified in Section 2.1, flames can emit electromagnetic radiation at different wavelengths, the details of which depend on the local environment within the flame. In the case of hydrogen flames, the absence of carbon leads to fewer chemical species to emit radiation. Indeed, there are only two primary sources of radiation: OH* luminescence in the ultraviolet range and excited H_2O* in the infrared range which also encroaches into the deep red part of the visible spectrum. In combination, hydrogen flames have historically been described as invisible [3] or nearly invisible [8]. However, the visibility of emissions from a flame is dependent on the lighting conditions from other sources.

Standards Australia TR 15916 (*Basic considerations for the safety of hydrogen systems*, 2021) describes hydrogen flames as “practically invisible in daylight”. This is consistent with widely reported observations [16]. On that basis, any scenario where there is potential for human interaction with a hydrogen flame requires additional control measures, such as making the flame more visible.

Notwithstanding the near-invisible nature of hydrogen flames, in the presence of impurities, various flame colours have been reported. In particular, orange colouration is widely reported, such as shown in Figure 2, which is attributed to the presence of sodium in the ambient air at low concentrations (refer Section 2.3). A reddish flame colour has also been reported due to a combination of other metal ions, including iron [2]. In general, the presence of metallic species in flames result in strong visible light signals from luminescence of the metal ions [17]. Red, blue/green, yellow, and orange flames are observed by introduction of strontium, copper, sodium, and calcium, respectively [18,19,20]. While the presence of impurities can be useful in improving the visibility of an otherwise colourless flame, reliance on the presence of said impurities may not be a sufficient robust control measure to ensure flame visibility.

Figure 2: Hydrogen cooker from Northern Gas Network’s demonstration project [21].

The OH*, H_2O* and metal spectra in hydrogen flames are widely reported and well understood. However, there have also been some observations of blue continuum of light from hydrogen flames. The precise origin of the blue continuum has been attributed to molecular hydrogen, monatomic hydrogen, and OH* radicals, though remains speculative [8,22].

In light of the preceding discussion, hydrogen flames have been experimentally observed to be a range of colours, with blue, orange, and red being the more commonly observed [8]. Red hydrogen flame features have been observed in gas turbine jet burners [2], as well as in jet in coflow burners [23], in both cases, impurities were cited as the primary cause for the reddish appearance. Similarly, in a swirl burner operating on 100% hydrogen fuel, a reddish flame was observed, with particular reference to vibrationally excited water molecules as the origin [24]. Other observations of turbulent hydrogen flames have attributed the reddish flame colour to the H-alpha transition of free hydrogen atoms that have not participated in the combustion process [17]. More recent experimental campaigns have noted reddish or orange colouration in hydrogen/nitrogen flames, again citing vibrationally excited H_2O as the primary cause [23]. The presence of alkali metals in hydrogen flames was studied photometrically, with sodium noted to produce significant luminescent effects at very low concentrations of addition to the hydrogen/nitrogen/oxygen flames [19,20]. Experiments using hydrogen of the same purity at different locations have resulted in different observations of the hydrogen flame colour [2,25]. The implication is that the ambient concentrations of chemically or thermally excitable species varies enough with location to result in distinct changes in flame colour, however, these changes have not been quantified. Premixed hydrogen flames tend to result in the bluish hue more so than the non-premixed flames, which appear to be more dominated by the reddish-orange, especially in laminar conditions [2]. Differences in residence time of the surrounding air and the flame results in less thermal excitation of the other radicals in the turbulent cases, as opposed to in the laminar cases [26,27]. Although experiments in low light conditions result in flames that are readily visible regardless of their unique colourations [2], different ambient lighting levels have also been noted to influence the visibility of hydrogen flames [8].

The overall visibility of hydrogen flames is influenced by a number of conditions that are not well quantified. However, introduction of other species to the flame can have significant effects on flame visibility. Addition of toluene to hydrogen flames has shown an increase in both visible light and in radiative heat transfer in a jet-in-hot coflow configuration, due to the production of soot and soot precursors [14,15]. Similar observations have been noted in hydrogen/methane blended flames, whereby increasing proportion of methane in a jet flame results in a more visible flame [28]. However, addition of hydrocarbons into a carbon-free flame increases harmful carbon-based emissions, which can be detrimental to the goal of carbon-free emissions. Doping of hydrogen flames with some hydrocarbon fuels has shown some reduction in the NO_x produced by pure hydrogen flames, balancing out some of the emissions issues [29]. Hydrogen flames have also been investigated in conjunction with biofuels to increase flame luminosity as well as radiative heat transfer properties, although quantification of the visible light changes was not made in that study [15]. Doping of hydrogen flames with alkali metals has been investigated, with distinct changes in flame visibility through addition of minor amounts of sodium, strontium, and calcium to the flame [20]. This suggests that artificial addition of metals to the fuel stream could greatly benefit the visibility of the flame, without the drawbacks associated with hydrocarbon additives, however, the practicality of this has not been investigated.

In summary, whilst hydrogen flames may be considered “invisible”, there are contributions of light from well-established molecular and radical species that will give a flame a faint red (and potentially blue) colour. In real-world scenarios, the presence of sodium may dominate and result in an orange colour. The extent of the colouration and how bright it appears is a complex function of a variety of factors, which are not well characterised in the uncontrolled scenarios encountered in typical domestic installations.

2.3 ATMOSPHERIC SODIUM DISTRIBUTION AND DETECTION

As discussed in previous sections, a distinct orange colouration because of sodium in flames has been reported widely. The presence of sodium in the air (typically in sodium chloride and sodium sulphate) is attributed to two main sources: sea salt aerosols (SSAs) and industrial production pathways [30,31,32]. Despite the significant contributions of industrial processes to atmospheric sodium content noted within previous studies, the orange colouration observed in hydrogen flames has been noted in experiments based in cities with minor industrial presences [32,33,34]. As such, the distribution mechanisms of SSAs are of interest to evaluate the prevalence of sodium in appliances. Importantly, most previous work on SSAs is in the context of corrosion due to chlorides rather than specifically sodium for flame colouration [35]. Due to the different chemical processes involved between corrosion and flame chemistry, the findings may have some distinct differences. Nonetheless, Figure 3 gives an example of the salinity distribution across Australia from previous work on corrosivity [31].

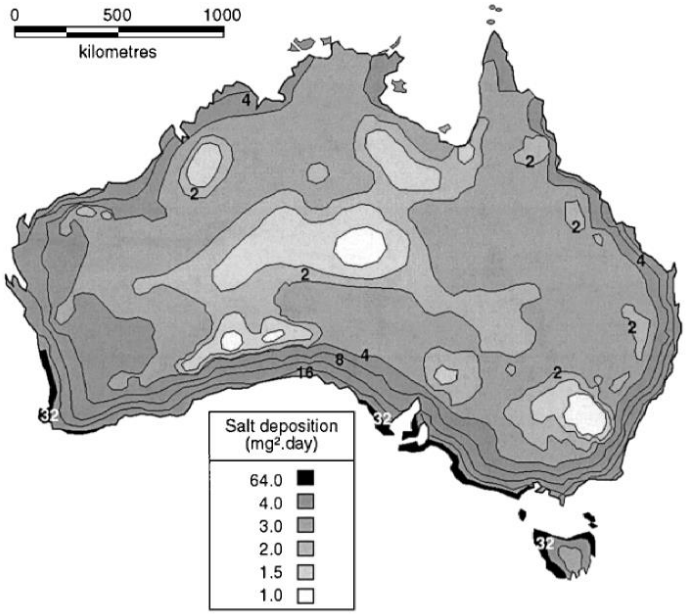

Figure 3: Salinity map of Australia [31].

Although the relevance of transport mechanisms for the distribution of SSAs inland is more pertinent to this project, it is insightful to understand the principal production pathways of SSAs. The production of SSAs is driven primarily through wind conditions at the surface of the ocean, whereby waves with whitecaps (foam) are formed, allowing transport of saltwater droplets into the atmosphere by either convection or turbulent transport [30]. However, additional influences beyond wind factors contribute towards the development of whitecap regions, including the local topography of the seabed, shipping routes, rainfall, and underwater currents [30,31]. A second major method of SSA production is bubble formation, which can be from a number of conditions, most notably through the breaking of larger scale waves which then produce bubbles [30]. Geographical features are therefore an important factor to consider as part of the overall distribution of SSAs inland, alongside the local weather conditions. It should be noted here as well that SSAs have a significant influence over climate change parameters, which will have an impact on future distributions of atmospheric sodium [30].

Transport of sea salt aerosols has been assessed in detail [30]. Wind is both the primary producer of the whitecaps that allow SSA production, as well as the principal transport method [30]. The marine atmospheric boundary layer governs the entrainment of SSAs via large scale convection processes and/or through turbulent transport [30]. Similar to the production pathways for SSAs, the marine boundary layer is dependent on both the local weather conditions, and on the topology of the sea surface [30]. This can influence whether the overall flux of SSAs from the surface of the sea are transported effectively to make landfall, otherwise called dry deposition [30]. The process of dry deposition of SSAs on land is a marker of the presence of atmospheric sodium ions, and is estimated to contribute to 65% of the overall SSA removal from the ocean, however, only 1–2% of this mass proportion is retained in the atmosphere [33,34].

Models exist of sodium content around the world [31]. One such model accounts for the distribution of SSAs across South Australia in particular, based on meteorological data, alongside both marine and land measurements of atmospheric constituents [31]. The resulting spread indicates that there is transport of SSAs inland of appreciable amounts up to 50 km inland, which accounts for the majority of the Australian population, and hence domestic appliances [31,35]. The deposited SSAs within the 50 km region of the coastline varies season to season, as well as by location [35]. South Australia shows differences compared to both New South Wales and Queensland, where summer in the latter two states shows the highest proportion of deposited SSAs [35]. Comparatively, the presence of SSAs in South Australia is highest in the winter [35]. The implication here is that the coastal features, along with seasonal patterns, will influence the presence of sodium ions in the atmosphere, which may in turn affect whether hydrogen flames are visible.

To quantify the presence of atmospheric sodium, several methods are available to determine the composition of chemical constituents in atmospheric air including sodium ions. Laser-induced breakdown spectroscopy (LIBS) is the most reliable and repeatable method for determining the composition of an atmospheric gas sample [36,37]. LIBS involves the use of a high-power laser that vaporises a gas sample and dissociates the present molecules [36]. The resulting mixture emits light of certain wavelengths that can be used to identify the species present in the sample [36]. However, although this method is accurate, the setup is both complex and costly, and cannot be performed continuously to monitor changing sodium concentrations [37]. Similar issues are encountered using atomic absorption spectroscopy, which also relies on the use of optical diagnostics to identify gas composition, with the additional complexity of requiring high temperature gas conditions, such as in a flame or furnace [38]. A more feasible method is gas chromatography, whereby a gas sample composition is determined using a mass spectrometer [37,39]. Typical sampling methods require a tube through which some ambient water is condensed, which can have an impact on the ionic concentrations present within the sample, reducing the reliability of this method of composition determination for the purpose of identifying sodium [39]. Despite these challenges, it is still important to reliably measure the level of sodium in atmosphere, however, appropriate methods may not be practicable under many scenarios.

An important consideration in the assessment of the interaction of sodium with flames is the chemical state of the sodium. It is known that the interaction of metal atoms with flames that lead to light emission is dependent on whether the metal is introduced in atomic or ionic (solution) phase [40]. Similarly, the humidity is known to influence sea salt aerosols [41]. In combination, it is known that the concentration of sodium alone is not expected to be the only factor to affect flame colour, and hence any measurement of SSA would need to take this into consideration. Thus, many of the existing techniques may not be reliable in predicting flame colouration, hence the need for experimental work.

3 Experimental Setup

3.1 BURNER DESIGNS

3.1.1 Jet burner

The jet burner was a simple jet made from stainless steel tubing: the outer diameter was 3.18 mm and inner diameter of 1.8 mm. It was operated in non-premixed operation (i.e. only fuel through the jet). Using a mass flow controller (*Alicat* brand) the flowrate was fixed at 1 SLPM (standard litre per minute) in all cases, consistent with the Phase 1 experiments.

The laminar nature of the flame makes it susceptible to draughts. Although for most testing indoors this was not an issue, to enable testing outdoors, an enclosure was made to avoid impacts of breeze. The enclosure did not affect the results (refer Section 4.1.1).

3.1.2 Hydrogen cooktop

An *Electrolux* brand hydrogen cooktop (single burner) was used, and is the only commercially designed hydrogen cooktop available in Australia. It operates with an inlet pressure of 2 kPa. The hydrogen burner used for this single burner cooktop is the same as used in the five-burner hydrogen cooktop at AGIG's "Hyhome" Hydrogen Gas demonstration home in Wollert, Melbourne: https://www.australiangasnetworks.com.au/hyhome

3.1.3 Domestic natural gas cooktop

A *Chef* brand naturally aspirated natural gas cooktop was used as an indicative contemporary open-flame burner encountered in a domestic setting. It is operated using reticulated gas in Adelaide. The burners of this cooktop are considered representative of most NG domestic cooktop burners.

3.2 DIAGNOSTIC TECHNIQUES

3.2.1 Spectrometer

The electromagnetic spectrum from the jet burner was recorded with an Ocean Optics USB650UV spectrometer. The input to the spectrometer was directed at the flame, with no collection optics. Integration time was constant at 500 ms. The number of samples collected was varied for each phase of the experiments, with a minimum of 100 samples per flame condition.

3.2.2 Camera

For the cooktops, the visual appearance of the flames was captured with Canon 6D camera, with a 50mm/f 1.8 lens. The white balance was specified as 5600 K, corresponding to the colour temperature of daylight.

During post-processing, the colour images were converted to greyscale using the Matlab `rgb2gray` function for the quantitative analysis of flame luminosity. According to the Matlab documentation: "`rgb2gray` converts RGB images to grayscale by eliminating the hue and saturation information while retaining the luminance." The mapping of the luminance (E) from the red (R), green (G) and blue (B) channels is based on the following weightings:

$$E = 0.299\,R + 0.587\,G + 0.114\,B$$

This conversion is consistent with the International Telecommunication Union Recommendation (ITU-R) for television broadcasting service, BT.601-7 [42].

3.3 VARIABLES

3.3.1 Fuel

The hydrogen fuel was N5 grade (>99.999% hydrogen), sourced from BOC (Ultra-High Purity, Gas Code 240). A cylinder regulator was installed and set to 200 kPa. Additional pressure regulators were installed upstream of the hydrogen cooktop to reduce the inlet pressure to 2 kPa.

3.3.2 Air

All hydrogen flames are non-premixed, relying on ambient air (no premixing or entrainment upstream of the burner exit).

3.3.3 Environment

Experiments were performed in the Adelaide area in South Australia, during the months of October and November 2024. As noted in Section 2.3, the extent of sea salt aerosols (SSA) is seasonal — higher sodium may be present during winter.

The primary test location was a domestic dwelling in Fulham Gardens, South Australia. The sea (Gulf St Vincent) is approximately 1200 m to the west of the dwelling. These tests were mostly performed in the garage, with all doors closed; however, due to openings around the roller doors, ventilation from outside was plentiful, especially on windy days. No heating, cooling, or mechanical ventilation was used, such that the environment is uncontrolled (beyond changes in local weather).

Additional tests were performed both outside and inside the Fulham Gardens dwelling and another dwelling in the Adelaide foothills (Hope Valley), as well as outside on the foreshore of West Beach.

Temperature and relative humidity were measured using a commercially available thermometer/hydrometer, and complemented by observations from the closest Australian Government Bureau of Meteorology weather station. The primary test location relative to Bureau of Meteorology station is shown in Figure 4.

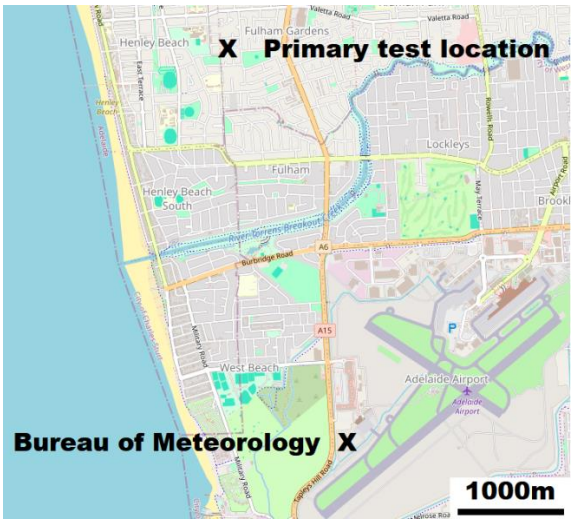

Figure 4: Primary test location relative to sea and Bureau of Meteorology station.

3.3.4 Lighting

The visual appearance of flames is dependent on the ambient lighting. In the context of real-world applications, this would be an important consideration. However, for the purposes of quantifying the visibility, the focus was on the underlying light emissions. On this basis, measurements were made in a darkened room and with a dark background.

For comparative purposes, some photographs were also taken with sunlight and/or room lights on. Efforts were made to normalise to account for these effects; however, the visual appearance of the flames is subjective, and thus care should be taken in interpreting the results.

4 Results and Discussion

4.1 SIMPLE OPEN JET FLAMES

4.1.1 Spectrometry measurements

Figure 5 shows a photograph and schematic diagram of the experimental configuration of the simple jet burner and the spectrometer. The entrance to the spectrometer was aligned to the jet centreline, 10 mm above the jet exit plane, and 15 mm radial distance from the jet centreline.

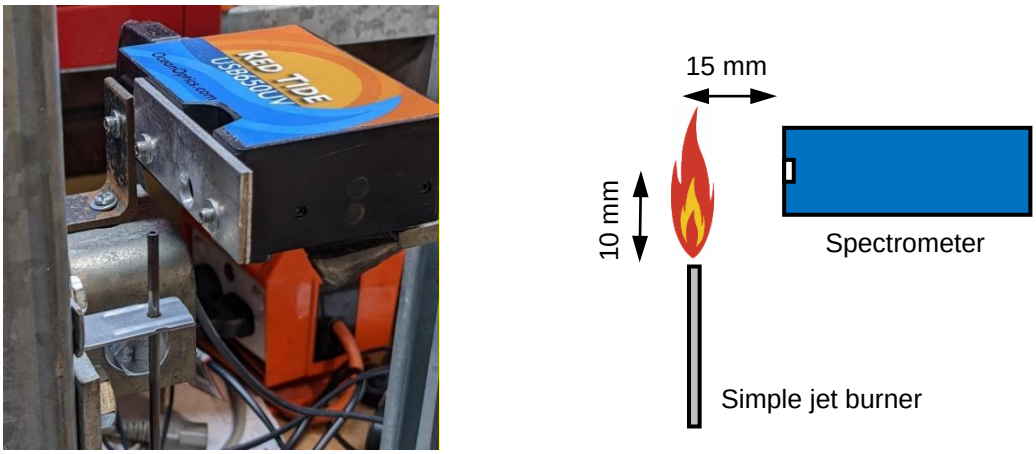

(a) Photograph (b) Schematic diagram (side view)

Figure 5: Simple jet and spectrometer experimental configuration.

The spectrometer was aligned with the flame and 100 scans were recorded, each with a 500 ms integration time. A sample spectrum — with 20 scans instead of the usual 100 scans — is shown in Figure 6 (20 scans are shown to demonstrate the variability, but not overwhelm with too many lines). Figure 6(a) shows the full range collected by the spectrometer and Figure 6(b) provides a more focussed view of the peak around 310 nm.

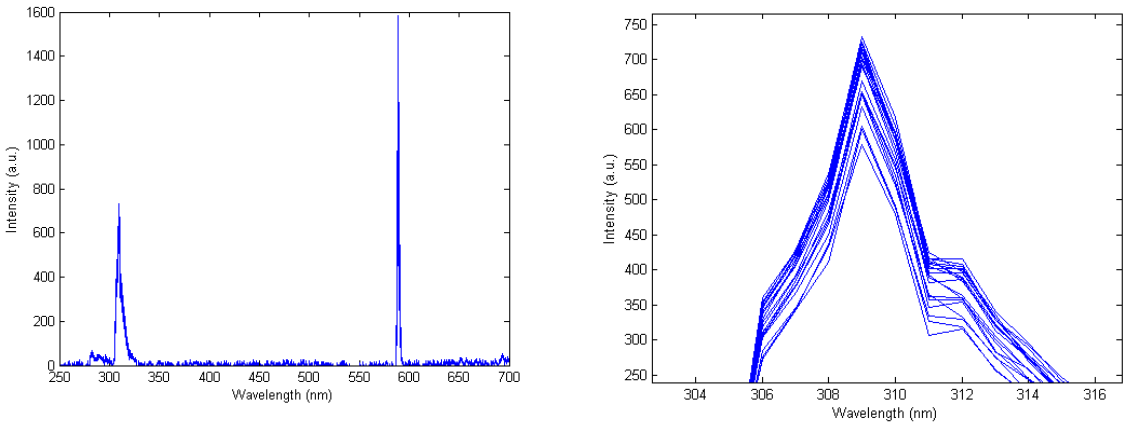

(a) Full spectrum (b) Narrowband spectral range

Figure 6: Example hydrogen flame spectrum. 20 individual spectra scans are shown.

Two distinct wavelengths are visible in the spectrum in Figure 6(a): a peak at 309 nm and another at 589 nm. The peak at 309 nm is attributed to OH* luminescence, and the peak at 589 nm corresponds to sodium.

The 20 individual spectra depicted in Figure 6(b) show some variation in the intensity between each integration period. However, the peak wavelength is consistently at 309 nm. The variation in the intensity appears as “flickering” when viewing the flame. The colouration of the flame is highly inconsistent, but is mostly statistically stationary over the total integration period of the spectrometer (100 integrations, each 500 ms).

Based on the spectral location of the peaks, the localised peak intensity can be identified. Moreover, because multiple scans are recorded, the standard deviation of the peak intensities can be determined. This gives a measure of the variability in the signal, due to fluctuations in the flame.

The absolute intensity of the peak is a function of the distance between the flame and the spectrometer, as well as the alignment of the spectrometer with the flame. The intensity is sensitive to these effects. To minimise the influence of misalignment between tests, the ratio of the two peaks is calculated (as the intensity will affect both wavelengths in the same proportion). The peak at 309 nm (due to OH* luminescence) is a measure of the reaction zone intensity. For these types of flames, the OH* intensity can be considered constant. Therefore, any change in intensity is a result of flame fluctuation. By normalising the peak at 589 nm by the peak at 309 nm, the relative intensity of sodium (Na*) can be determined.

Figure 7 shows an example of the automated procedure to identify the peak (and standard deviation) of the OH* and Na* signals. The relative intensity of peak Na* to OH* is 1.6 (=1101/676). Although this number is a non-dimensional ratio, it can be used to compare the relative intensity of sodium between different flame conditions. It should also be noted that the ratio itself is unique to the spectrometer used in this study. It is insightful to compare relative trends and can be used quantitatively within this report, but the exact value of the ratio between peaks would change depending on the calibration of a different spectrometer.

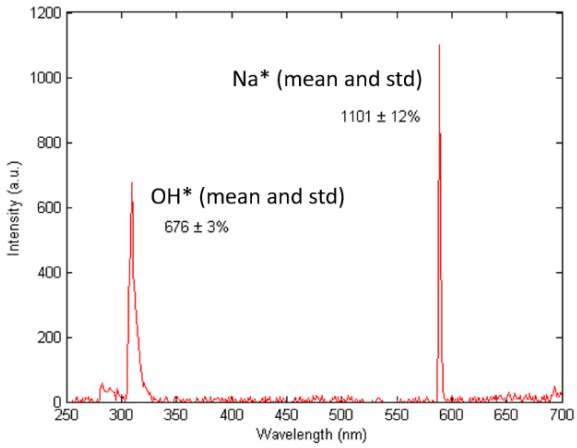

Figure 7: Example labelled spectrum.

In general, the OH* signal is nearly constant. In Figure 7, the standard deviation in the OH* signal is 3%, whereas the Na* signal fluctuates by 12%. This is consistent with the fluctuating nature of sodium coming from the air, such that its intermittency is higher — and is visually apparent when observing the flames.

Notwithstanding the inherent variability due to fluctuation in the level of sodium, the average of 100 scans is sufficient to provide a statistically meaningful mean value. This ensures repeatability to within approximately 10% of the mean. A further measure of repeatability is verified by measurements with and without the enclosure. The agreement in the measurement is also within 10% when comparing the mean Na/OH ratio from two consecutive averages, each of 100 scans.

4.1.2 Spectrometry results

Figure 8 shows the Na/OH ratio from measurements from the simple jet burner over a fortnight period, morning (~7am) and evening (~9pm) each day. These were all collected at the one location (garage in Fulham Gardens, Section 3.3.3). Spectrometry measurements under different conditions are presented later in this report.

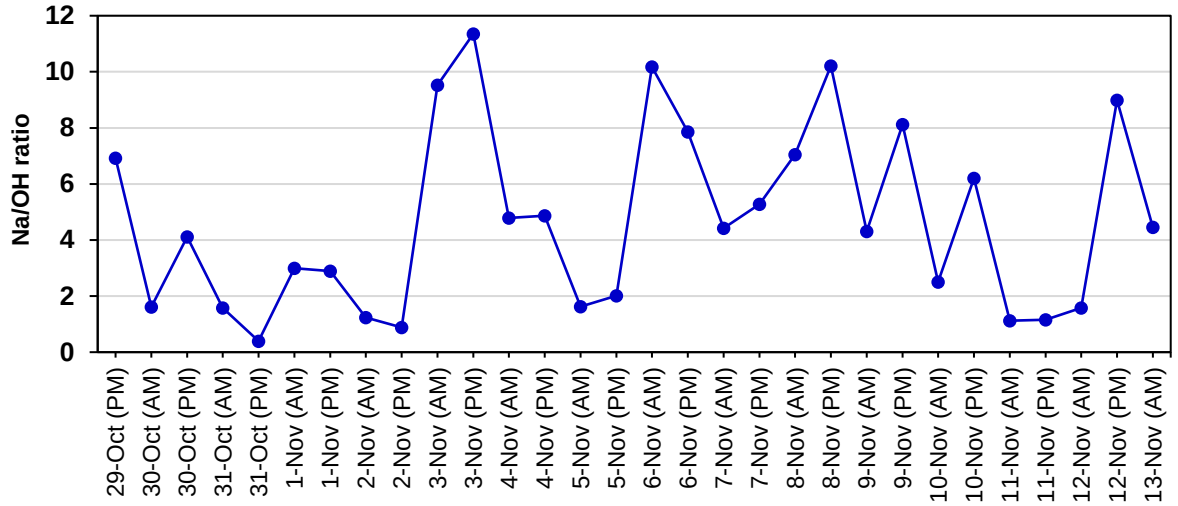

Figure 8: Normalised sodium intensity in simple jet burner over a fortnight period.

The normalised sodium intensity from the simple jet burner (Figure 8) varies significantly between testing times, varying by an order of magnitude between the minimum and maximum Na/OH ratio (minimum 0.4, maximum 11.4). To demonstrate the distribution of Na/OH ratio, Figure 9 presents a histogram of the frequency for the 30 samples reported in Figure 8. The lowest Na/OH ratio band (0-2) accounts for the highest frequency, although there are many samples across the range of the Na/OH levels. Noting the repeatability of the measurements is better than 10% (Section 4.1.1) and that all controlled parameters are constant, the variability is mostly attributed to different weather conditions between tests.

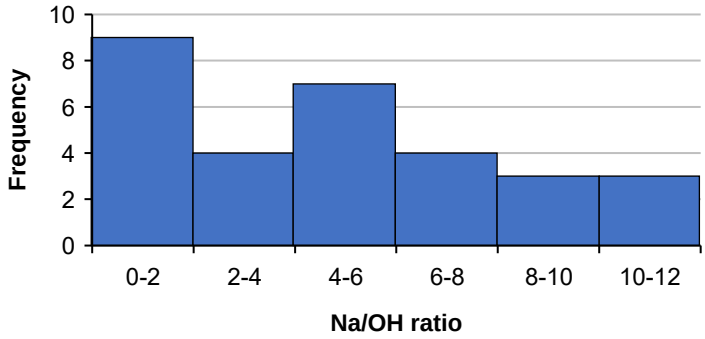

Figure 9: Histogram of Na/OH ratio for data presented in Figure 8.

4.1.3 Spectrometry discussion

To complement the data presented graphically in Figure 8, Table 1 reports the Na/OH ratio for each day, along with selected weather observations (recorded as part of the test, and sourced from the nearest Bureau of Meteorology site).

Amongst the various data reported in Table 1, it appears as though the Na/OH ratio is most correlated with wind direction. To demonstrate the influence of wind direction, Figure 10(a) shows the Na/OH ratio (as distance from centre) as a function of wind direction. Each data point represents the Na/OH ratio and the corresponding wind direction (note that wind speed is not captured in this figure). Note that Figure 10(a) includes all spectral measurements at different locations, and with/without the enclosure. Notwithstanding that the most common wind direction is in the south-western quadrant (typical for Adelaide) it is also noted that the general sodium intensity is greatest when the wind has a predominant westerly component — in Adelaide, this corresponds to wind that has passed over the sea. This effect is reinforced in Figure 10(b) which shows the average Na/OH ratio in each wind direction, for the measurements reported in Table 1, with the origin of the vectors indicating the location of the primary test location. The vectors pointing with a westerly component, which are the longest, indicate the wind direction that brings air from over the sea to the test location (i.e. arrowheads depict direction, rather than air flow).

Table 1: Daily measurements of sodium-to-OH ratio (Na/OH) and weather conditions.

Date	Na/OH	Measured		Bureau of Meteorology					
		Temp (°C)	Rel Hum (%)	Temp (°C)	Dew Pt (°C)	Rel Hum (%)	Wind (dir)	Wind Spd (km/hr)	Rain since 9am (mm)
29-Oct (PM)	**6.9**	-	-	19.9	9.5	51	SSW	19	0
30-Oct (AM)	**1.6**	-	-	15.3	6.1	54	ENE	6	0
30-Oct (PM)	**4.1**	-	-	18.7	12.9	69	SSW	11	0
31-Oct (AM)	**1.6**	-	-	13.7	9.4	75	SE	7	0
31-Oct (PM)	**0.4**	-	-	16.8	10	64	S	26	0
1-Nov (AM)	**3.0**	-	-	12.3	5	61	ESE	11	0
1-Nov (PM)	**2.9**	-	-	15.7	5.6	51	E	19	0
2-Nov (AM)	**1.2**	16.9	35	18.8	-0.1	28	NE	17	0
2-Nov (PM)	**0.9**	28.1	22	32	2.1	15	N	24	0
3-Nov (AM)	**9.5**	18.9	52	16.4	10.9	70	SW	20	0
3-Nov (PM)	**11.4**	20.3	47	16.6	10	65	SSW	15	0
4-Nov (AM)	**4.8**	17.7	52	14.9	9.3	69	NE	6	0
4-Nov (PM)	**4.9**	20.9	46	17.1	10	63	SSW	13	0
5-Nov (AM)	**1.6**	17.1	50	14.1	8.5	69	CALM	0	0
5-Nov (PM)	**2.0**	23.1	48	25.3	9.6	37	NE	35	2
6-Nov (AM)	**10.2**	21.3	60	18	15.1	83	W	6	2
6-Nov (PM)	**7.9**	20.5	56	17.1	12.8	76	WSW	30	0
7-Nov (AM)	**4.4**	17.3	57	13	9.3	78	NNE	11	0
7-Nov (PM)	**5.3**	19.3	52	15.9	9.1	64	SW	24	0.2
8-Nov (AM)	**7.0**	17.4	61	14	12.2	89	SW	30	0.6
8-Nov (PM)	**10.2**	19	49	16	8.5	61	SSW	17	0
9-Nov (AM)	**4.3**	16.7	50	14.9	5.7	54	NE	17	0
9-Nov (PM)	**8.1**	19.5	49	17.1	9.3	60	SSW	15	0
10-Nov (AM)	**2.5**	16.2	56	16	9.9	67	CALM	0	0
10-Nov (PM)	**6.2**	22	48	20.6	9.5	49	SE	17	0
11-Nov (AM)	**1.1**	19.1	59	16.9	14.9	88	CALM	0	1.4
11-Nov (PM)	**1.2**	26.2	43	24.8	12.7	47	NE	20	0
12-Nov (AM)	**1.6**	21.1	53	19	12.7	67	NNE	13	0
12-Nov (PM)	**9.0**	21.1	62	18	14.3	79	SSW	28	0
13-Nov (AM)	**4.5**	17.4	58	16.4	8.4	59	SSW	24	0

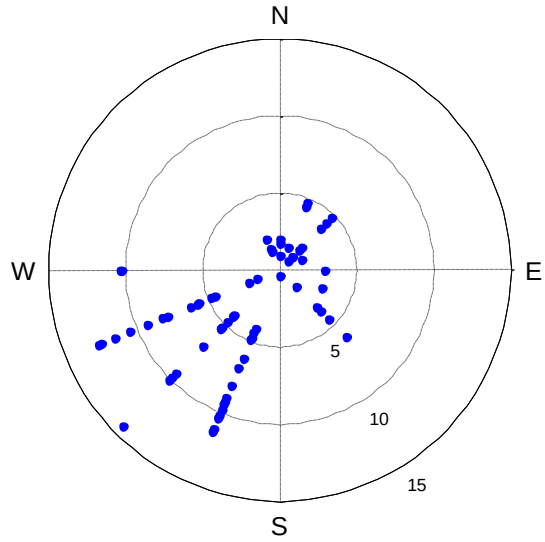

(a) Each point shows wind direction, and distance from the origin represents the Na/OH ratio (values on radii of the circles: 5, 10, 15). Note: includes all spectral measurements at different locations, and with/without the enclosure.

(b) Length of each vector indicates average Na/OH ratio for each wind direction, overlaid on map. Centrepoint is primary location. Data only includes measurements at the primary test locations, consistent with the data presented in Table 1.

Figure 10: Sodium (Na/OH ratio) as a function of wind direction.

To demonstrate the correlation between Na/OH ratio and weather conditions other than wind direction, Na/OH ratio is plotted as a function of wind speed, temperature, and relative humidity in Figure 11. Unlike the apparent trend found in Figure 10, there does not appear to be a strong correlation of Na/OH with wind speed, temperature, or relative humidity as can be seen by the almost random scattering of measurement points in each of the three graphs in Figure 11. The results imply that wind speed, temperature, and relative humidity have minor influence on the visibility of hydrogen flames under real-world conditions, compared with wind direction. Although wind speed may be expected to increase the formation of SSA, the experimental data does not seem to support this assumption. Noteworthy is that the data at the highest temperature and lowest humidity correspond to days with a northerly wind direction — however, decoupling those effects from wind direction would be imprecise from the number of data points available.

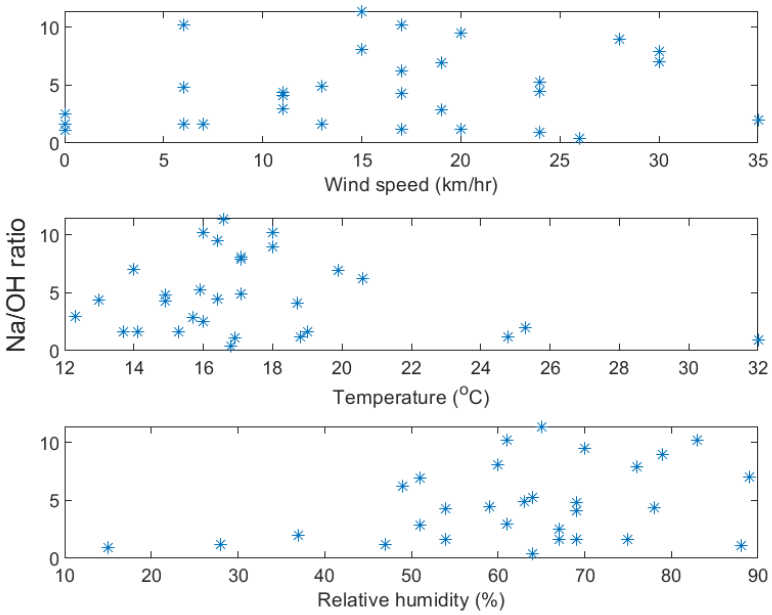

Figure 11: Sodium (Na/OH ratio) as a function of wind speed, temperature, and relative humidity.

4.2 COOKTOP FLAMES

4.2.1 Hydrogen cooktop photographs

Figure 12 shows a diagram (side view) of the configuration of the camera and the cooktop, with the viewing angle intended to be similar to typical usage for domestic cooking.

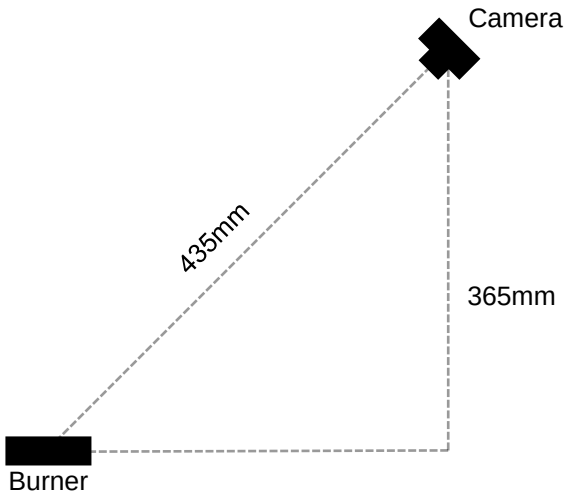

Figure 12: Side view schematic showing location of camera relative to cooktop burner.

Typical photographs of the flames are shown in Figure 13. These two photographs are taken under the same operating conditions (hydrogen flowrate, camera settings, etc.) – the only difference being atmospheric conditions. Based on the spectrometry measurements from the jet burner, the Na/OH ratio at the time of the photographs in Figure 13(a) and Figure 13(b) were 0.4 and 11.4, respectively.

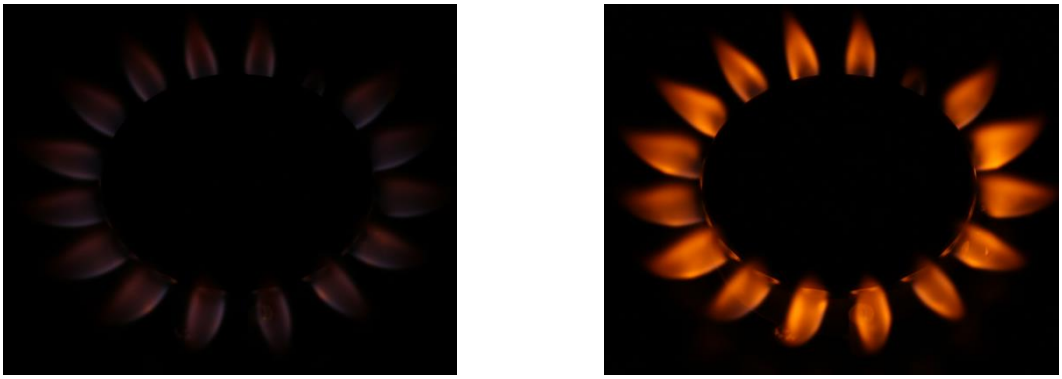

(a) 31st October (Na/OH = 0.4)

(b) 3rd November (Na/OH = 11.4)

Figure 13: Example hydrogen flame photographs on cooktop on two different days. All controlled parameters held constant between the two photographs.

The significant visual discrepancy between the two photographs in Figure 13, and the apparent correlation with the Na/OH ratio, reinforces the expectation that hydrogen flame appearance is strongly related to the sodium level in the air. The results from Figure 13 (in conjunction with the inter-day spectrometry data in Figure 8) indicates that the visual appearance of hydrogen flames is not consistent under all conditions.

4.2.2 Photograph analysis

Whilst visual inspection of the photographs is insightful, to enable a more quantitative analysis, an image processing algorithm was used to extract the luminosity from the photographs:

(a) Load image.

(b) Crop and downscale.

(c) Convert to greyscale.

(d) Check if image is saturated (if so, then disregard and flag an error).

(e) Remove dark-charge (i.e. remove residual pixel intensity in the absence of light).

(f) Set threshold (to mask parts of image <10% of the peak pixel intensity).

(g) Calculate total intensity and average pixel intensity.

Figure 14 shows an example of an image at key steps of the process.

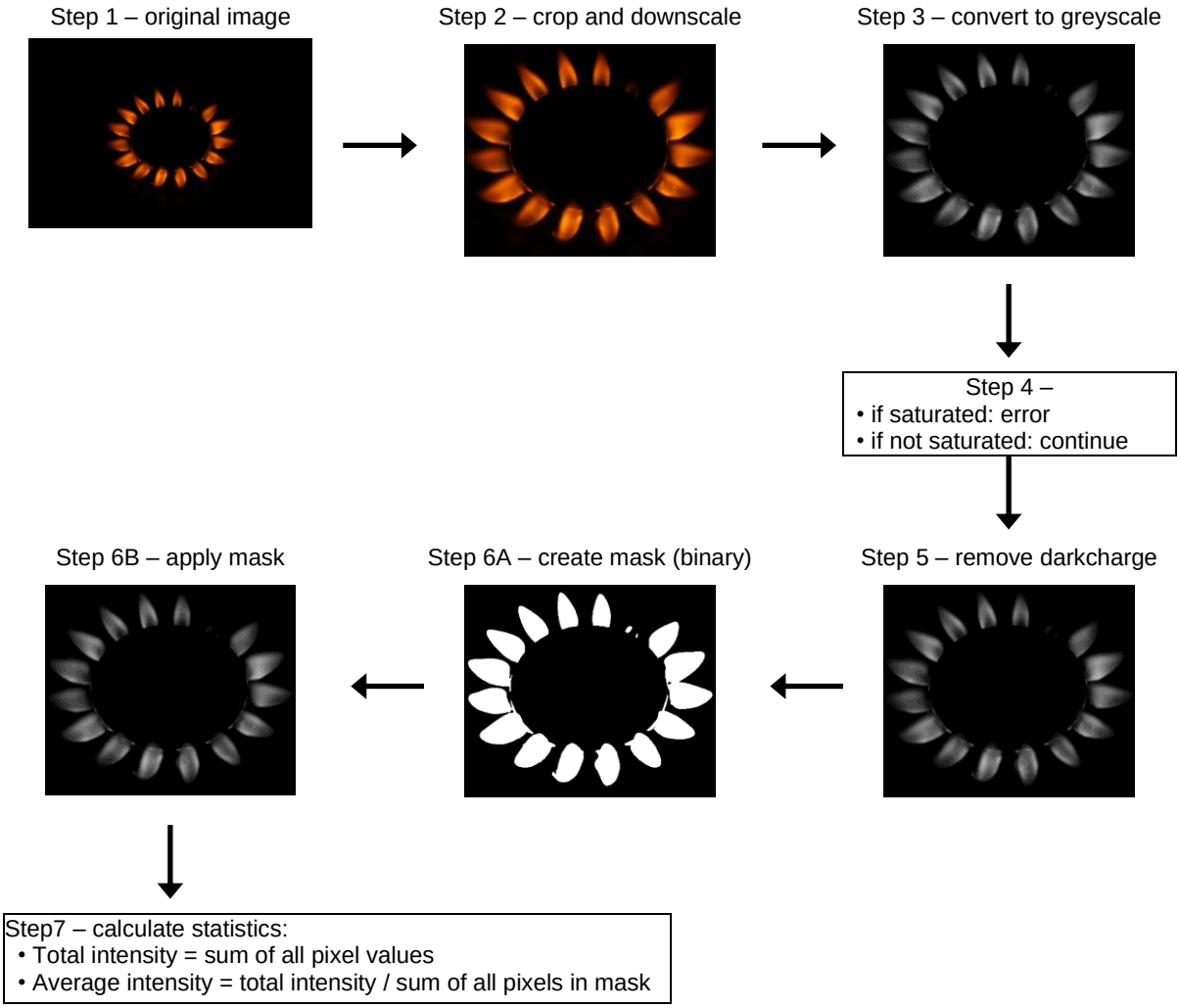

Figure 14: Image processing flowchart.

Although a conversion between different camera settings based on their exposure value could be performed, to avoid any potential inconsistencies, all photographs presented in this report were recorded in a darkened room, with the following camera settings: 1-second exposure time, f-number of 8, and ISO sensitivity of 400. This exposure value was found to not lead to saturation for any of the flame photographs (Step 4).

4.2.3 Natural gas cooktop photographs

Photographs of the natural gas flames on the cooktop flames are shown in Figure 15, along with a comparison against the hydrogen flame (the most luminous, representing the "brightest" hydrogen flame collected). The camera was positioned at the same distance and angle relative to the burner. The geometry of the burners was quite similar, but with a slightly different flame shape. Figure 15(a) and Figure 15(b) are for natural gas and hydrogen, respectively, with the camera sensitivity set to ISO 400. Both flames are readily identified visually, which is exacerbated by the dark background and the ISO sensitivity providing high pixel intensity. Halving the camera sensitivity to ISO 200 is shown in Figure 15(c) and Figure 15(d). With lower sensitivity, the natural gas flame remains readily visible, but the hydrogen flame intensity appears significantly reduced.

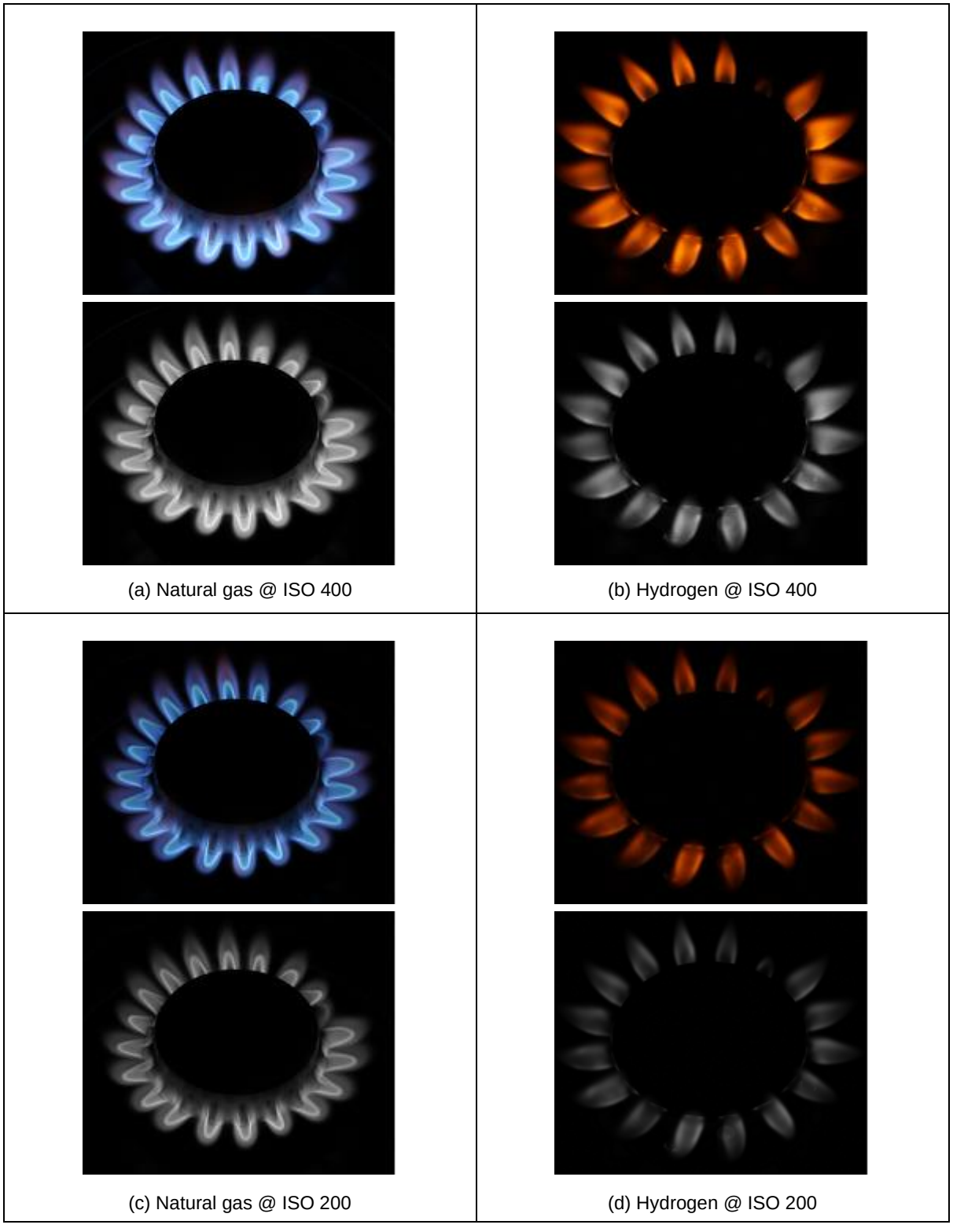

(a) Natural gas @ ISO 400

(b) Hydrogen @ ISO 400

(c) Natural gas @ ISO 200

(d) Hydrogen @ ISO 200

Figure 15: Example cooktop flame colour photographs and greyscale images. All controlled parameters held constant between the photographs, except for ISO sensitivity.

4.3 PHOTOGRAPHS UNDER DIFFERENT LIGHTING CONDITIONS

All photographs shown in Section 4.2 were taken in a darkened room (near-zero lighting). However, the appearance of the flame under more realistic cooking conditions is expected to be different. To account for this, Figure 16 shows photographs of flames under common kitchen lighting. The exposure value of these images is EV = 6 (corresponding to a common “home interiors” level). Notwithstanding the slightly darker background colour of the natural gas cookstove, the blue colouration of the natural gas flame appears more pronounced than the hydrogen cooktop. The Na/OH ratio at the time of these tests was 4.2, which is a relatively common mid-level of sodium. The Na/OH ratio is often less than this, and hence the colouration of the hydrogen flames could reasonably be expected to be less than depicted in Figure 16.

Even under the most amenable conditions, the hydrogen flame is less visible than natural gas flames. Changing background might give a different relative perspective, but noting that the hydrogen flame is barely visible with a black/dark background, the relative appearance of a blue versus orange flame against a white background becomes unimportant because the flame will necessarily be difficult to see.

(a) Hydrogen cooktop flame

(b) Natural gas cooktop flame

Figure 16: Photographs of cooktop flames under well-lit conditions. Exposure value EV = 6 (1-second exposure time, f/8, ISO 100). The corresponding Na/OH ratio was 4.2.

4.4 CORRELATION BETWEEN SPECTROMETRY AND PHOTOGRAPHS

Based on the image processing algorithm (Section 4.2.2), Figure 17 presents the (a) total and (b) average pixel intensity of the photographs of the hydrogen cooktop flames, as a function of the Na/OH ratio determined from the simple jet burner collected at the same time.

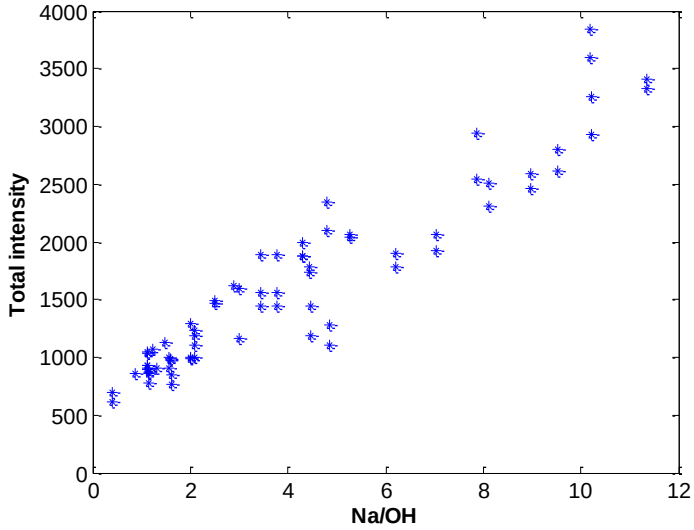

(a) Total intensity, calculated by sum of pixel values

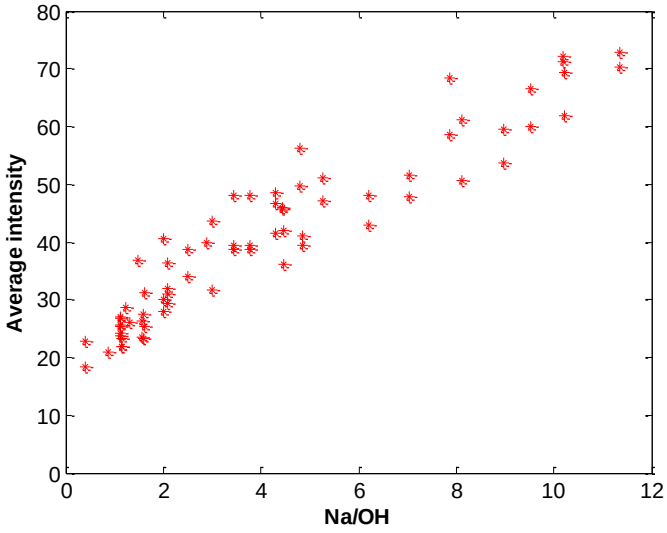

(b) Average intensity, calculated by total intensity normalised by number of non-zero pixels.

Figure 17: Total and average pixel intensity of hydrogen cooktop photographs as function of sodium-to-OH ratio from simple jet burner.

In both the total and average graphs in Figure 17, a near-linear correlation is apparent between the pixel intensity of the cooktop photographs and the Na/OH ratio in the simple jet flames. Although some deviation is noted from a perfect linear correlation, there is a general trend of increasing Na/OH ratio corresponding with higher intensity in the photographs. The correlation is approximately consistent between the total and the average intensity plots.

The natural gas flame has a different size, however, the average pixel intensity can be compared with the hydrogen flames. Because the natural gas flame colour is not strongly affected by the sodium, a single value can be calculated, and is depicted by the horizontal green line in Figure 18. The average pixel intensity in the natural gas flame is 108 units, well above any of the intensity values for any of the hydrogen flames. This provides an indication that hydrogen flames emit significantly less light than natural gas.

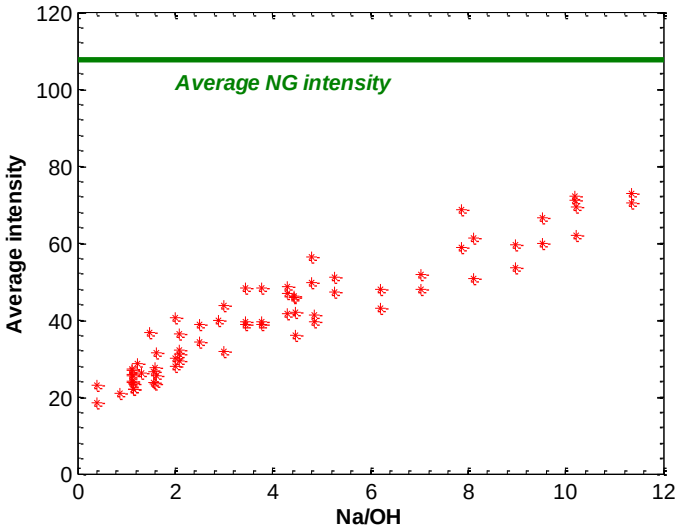

Figure 18: Average pixel intensity of cooktop photographs as function of sodium-to-OH ratio from simple jet burner: red markers indicate hydrogen flames, green line indicates natural gas flame.

4.5 SPECTROMETRY DATA AT DIFFERENT LOCATIONS

It was not practicable to transport the cooktop to different locations, especially under controlled conditions (dark and without effects of wind). However, the simple jet burner rig can be much better shielded from the wind, and the effects of ambient light are much less pronounced. Noting the good correlation between the intensity of the cooktop photographs and the Na/OH ratio (Section 4.4), a comparison of the Na/OH ratio at different locations can be used to infer the likely impact on cooktop flame appearance.

Noting the variation on an intra-day basis (Section 4.1) a direct comparison between all test locations is not viable, however, for each variation, measurements at the primary test location were recorded (typically before/after, and with very close agreement) – results presented in Table 2. The primary test location was a garage at Fulham Gardens (Section 3.3.3) with additional tests inside the main dwelling, and outdoors at the same address. Tests were made at a beach near the primary test location, and a dwelling in the Adelaide foothills approximately 25 km from the beach (tests performed both inside and outside).

Table 2: Sodium-to-OH ratio at various test locations.

Test location	Na/OH	Primary location (garage)
Primary location – indoors	1.8	5.3
Primary location – outdoors	12.5	10.5
Beach	14.2	4.8
Foothills – indoors	3.1	3.4
Foothills – outdoors	4.2	3.4

Data collected at the different test locations indicates that the garage reduces the Na/OH ratio compared with outside, and that testing indoors reduces the ratio even further. Testing near the beach significantly increases the Na/OH ratio. The results at the primary test location compared with the dwelling in the Adelaide foothills were quite similar, however, the two tests were several hours apart, and thus there may have been changes in meteorological conditions that could not be accounted for (noting that the wind direction at the primary location changed from a south-easterly to a south-westerly before/after the tests in the foothills.

Notwithstanding some nuances in the comparison of the Na/OH ratio between the test locations, it seems that except for the foreshore, the difference in location is less influential than the wind condition. However, this assertion is based on relatively sparse data and may be strongly dependent on the geographical location.

4.6 ANECDOTAL OBSERVATIONS

4.6.1 Effect of burner temperature

Based on previous work by the research team on cooktop burners operated on hydrogen, it was noticed that the orange colouration became more intense the longer the burner was operating. There are several mechanisms by which the increase in temperature may affect the flame colour. However, for the cooktop burner used in the current study, this observation was not observed and could not be replicated. It is hypothesised that the non-premixed design of the burner, coupled with the small diameter of the ports, ensures that the flame heat release occurs away from the burner surface. Figure 19 provides some supporting evidence, whereby thermal imaging indicates that after the burner was operating for 10 minutes, immediately after turning off the flame, the temperature of the burner cap is 130°C, and the hottest part of the burner is the ignition rod, at 154°C. Previous burner tests are likely to have achieved a significantly higher temperature of the burner.

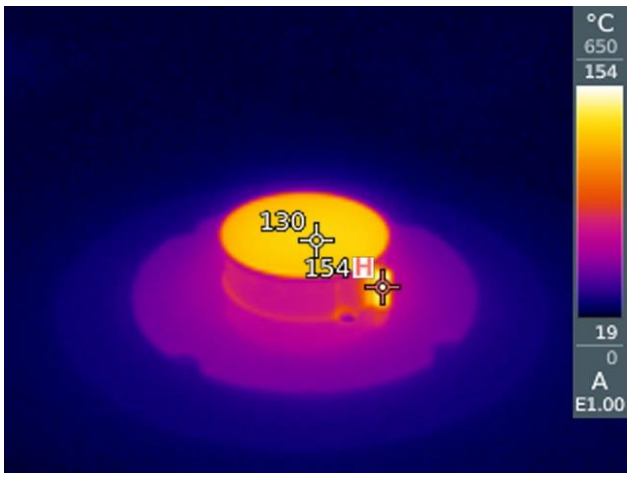

Figure 19: Thermal image of hydrogen cooktop burner immediately after flame turned off.

4.6.2 Overseas locations

During a research visit to a research laboratory in Saudi Arabia, despite being less than 1 km from the Red Sea, hydrogen flames in a laboratory were observed by one of the current authors to be completely free of visible sodium

emissions. Indeed, even in a darkened room, the flame could barely be seen. It is important to recognise that the laboratory was well isolated from the outside environment, in a “clean room” and with all fresh air thoroughly filtered and air conditioned. This indicates that in Australian settings with extensive HVAC and filtration, the sodium colourations presented in this report may be “most favourable” to leading to orange colouration — in other dwellings, the colouration may be significantly less.

4.6.3 Temporal response

The photographic images reported have been from 1-second exposure time, incorporating some level of time integration. However, during observation, the orange colouration is seen to be highly intermittent, giving the appearance of the flame flickering. To demonstrate this, videos were recorded of a hydrogen cooktop flame: one on a day with the Na/OH ratio of 7.9 and another day with a ratio of 1.6. Each frame from the video was extracted, and a single “flamelet” was identified — depicted by the green box in a sample frame in Figure 20. Using the algorithm described in Section 4.2.2 for just the selected flamelet, the average luminosity was determined for each frame, with the results presented in Figure 21. The luminosity was scaled to give an average of 1, shown by the horizontal red line. As shown in Figure 21(a) the intensity of the selected flamelet was often well below the average, but instantaneously the intensity would sometimes be an order of magnitude higher. These intense flashes may somewhat counteract the average lower intensity of the hydrogen flames, compared with natural gas (where average natural gas luminosity shown by green dashed horizontal line). However, these intense flashes are sporadic (16% exceed the intensity of the natural gas flame) and because they occupy much less of the visible area of the flame, are less noticeable than the constant blue colouration of a conventional natural gas flame. In comparison, Figure 21(b) shows the same measurements on a day with lower Na/OH ratio, where only 5% of the hydrogen flame instantaneous frames have an intensity above the average intensity of the natural gas flame.

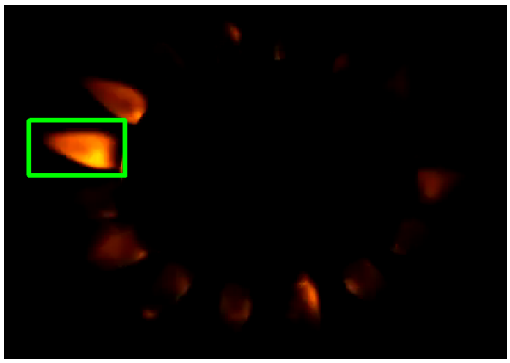

Figure 20: Sample frame from cooktop burner video. One flamelet indicated by green box.

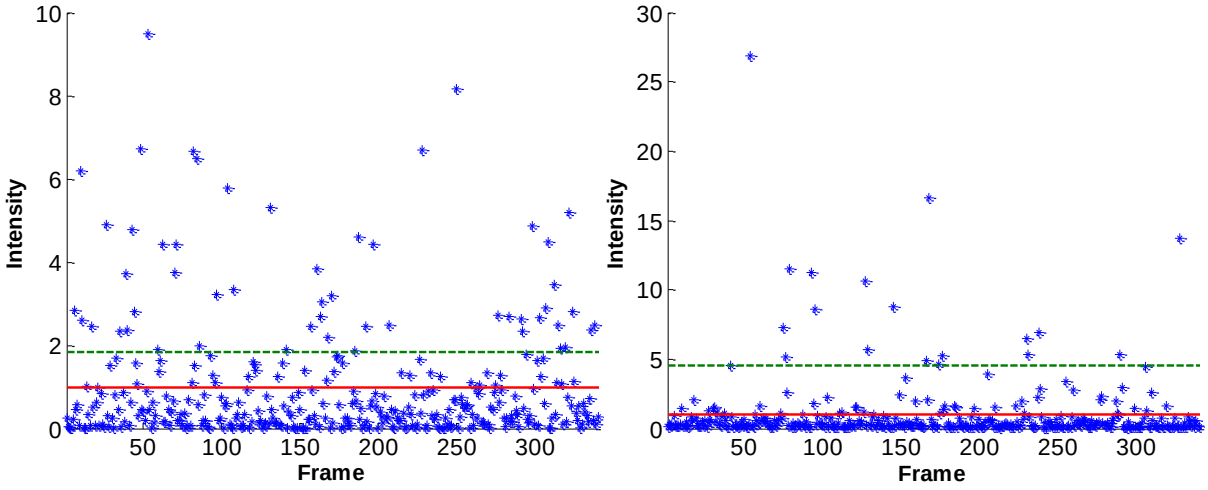

(a) Na/OH = 7.9

(b) Na/OH = 1.6

Figure 21: ***Intensity of one flamelet from each frame in two separate 12-second videos of a hydrogen cooktop burner – taken on different days (with corresponding Na/OH ratio as shown). Horizontal red line indicates the average luminosity (normalised intensity = 1). Horizontal green dashed line indicates the average luminosity of a natural gas flame.***

5 Conclusions

Hydrogen flames are known for being difficult to see depending on the circumstances in which they are installed, which poses a significant safety challenge if they are to be used in domestic settings where visual identification of a flame is important. Nonetheless, some hydrogen flames have been observed to be orange in colour in demonstration settings. When hydrogen flames are visible, this is generally via orange colouration attributed to the presence of sodium in the ambient air.

Based on the findings in the Phase 1 report under laboratory conditions, the visibility of hydrogen flames on a jet burner and cooktop have been investigated and compared with natural gas flames under real-world conditions through a combination of photography and spectroscopy. This report presents the influence of various factors in the real-world conditions on the visibility of hydrogen flames, including location, lighting, and weather condition. In brief, the key findings are:

(a) In general, hydrogen flames are less visible than natural gas flames under real-world conditions.

(b) The orange colour of hydrogen flames, due to the presence of sodium in ambient air, is variable under real-world conditions.

(c) Sodium in the ambient air displays a near-linear correlation with hydrogen flame luminosity — the higher the Na/OH ratio, the brighter the flame appears.

(d) Wind direction is the primary factor affecting hydrogen flame luminosity — air that has passed over the sea gives the most luminous flames. Wind speed, temperature, and relative humidity show comparatively less correlation to the luminosity.

(e) Difference in physical location (distance from sea, and indoors/outdoors) may be less influential than weather conditions in affecting hydrogen flame luminosity.

(f) The luminosity of the intermittent orange flamelet in cooktop hydrogen flames can be instantaneously an order of magnitude higher than the average luminosity.

6 Implications and Recommendations for Industry

The appearance of hydrogen flames continues to be an important factor in applications where visual flame detection is essential. Sodium content plays a significant role in the visibility of hydrogen flames, particularly in domestic settings. However, the factors that influence sodium levels in the local atmosphere and surrounding environmental conditions are only partially understood.

As evidenced through Section 4.1, sodium level in the ambient air varies significantly — changes in weather conditions being the primary cause, with other factors (e.g. location) also contributing. This indicates that consistent intensity of the orange colouration from ambient sodium cannot be achieved under real-world conditions. Although further testing could be conducted over a more extended duration and under a wider range of conditions (e.g. climatic, seasonal, and physical location) this report has evidenced that hydrogen flames are less visible than natural gas flames. Importantly, this was true under all tested conditions in a domestic setting, despite being in a favourable location near the sea (the source of sodium). Other test conditions are only expected to reinforce the concerns of low visibility. Consequently, relying on the presence of sodium in ambient air for flame visibility would be ill-advised. Reliable and distinctive flame visibility and colouration would require the introduction of non-ambient constituents to be introduced to the combustion process as a method for increasing flame visibility.

Hydrogen flames established on a cooktop exhibit less luminosity than natural gas flames under all lighting conditions. Even under the most favourable conditions for hydrogen flames (i.e. dark background with minimum lighting) and with moderate sodium in the air, some cooktop hydrogen flames are barely visible. It is expected that in other real-world domestic scenarios, hydrogen flames would be difficult to see. This suggests that alternative means to ensure indication of the presence of the flame would be necessary. This could be achieved through artificial addition of a colourant to hydrogen flames or some other form of visual indicator.

This Phase 2 report has presented results from a simple jet burner and a cooktop, and demonstrated that the luminosity of the two are linearly correlated. Both burners operate as a non-premixed flame. In Phase 1, partial premixing with forced air further lowered the flame luminosity. Partially premixing through entrainment has not been assessed in this project, but findings from other Future Fuels CRC projects it has been identified that there are many practical challenges with this type of configuration (e.g. flashback with burner turndown). Therefore, some alternative burner designs could be considered, but there is no evidence that these would provide a luminous flame in the absence of sodium.

Overall, the recommendations that stem from this extended investigation to real-world conditions is that orange colouration of hydrogen flames significantly varies due to the changes of sodium content in ambient air. The causes of the sodium change are ascribed to various factors, including weather conditions and geographical locations, which are challenging to control in real-world conditions. Given that cooktop hydrogen flames are much less luminous than natural gas flames, and the resultant enhanced luminosity from sodium is not consistent, it is not appropriate to rely upon flame visibility from ambient combustion as a safety measure for hydrogen appliances in a domestic setting without additional controls or appliance design measures.

7 References

[1] X. Zhu, A.A., Khateeb, W.L. Roberts, T.F. Guiberti. “Chemiluminescence signature of premixed ammonia-methane-air flames”, *Combustion and Flame* **231**, 111508 (2021). DOI: 10.1016/j.combustflame.2021.111508

[2] Y. Zhao, K.N. Soto Leytan, V. McDonell, S. Samuelsen. “Investigation of visible light emission from hydrogen-air research flames”, *International Journal of Hydrogen Energy* **44**, 22347-22354 (2019). DOI: 10.1016/j.ijhydene.2019.06.105

[3] A.G. Gaydon. “The Spectroscopy of Flames”, Second Edition, Chapman and Hall (1974). DOI: 10.1007/978-94-009-5720-6

[4] V.N. Nori, J.M Seitzman. “CH* chemiluminescence modeling for combustion diagnostics”, *Proceedings of the Combustion Institute* **32**, pp. 895-903 (2009). DOI: 10.1016/j.proci.2008.05.050

[5] M. Vanpee, R.J. Mainiero. “The spectral distribution of hydrogen flame continuum and its origin in hydrogen-nitric oxide flames”, *Combustion and Flame* **34**, pp. 219-230 (1979). DOI: 10.1016/0010-2180(79)90097-X

[6] J. Kojima, Y. Ikeda, T. Nakajima. “Basic aspects of OH(A), CH(A), and C_2(d) chemiluminescence in the reaction zone of laminar methane–air premixed flames”, *Combustion and Flame* **140**, pp. 34-45. DOI: 10.1016/j.combustflame.2004.10.002

[7] J.-M. Samaniego, F.N. Egolfopoulos, C.T. Bowman. “CO_2* chemiluminescence in premixed flames”, *Combustion Science and Technology* **109**, 183-203 (1995). DOI: 10.1080/00102209508951901

[8] R.W. Schefer, W.D. Kulatilaka, B.D. Patterson, T.B Settersen. “Visible emission of hydrogen flames”, *Combustion and Flame* **156**, pp. 1234-1241 (2009) DOI: 10.1016/j.combustflame.2009.01.011

[9] Y. Ding, D. Durox, N. Darabiha, T. Schuller. “Chemiluminescence based operating point control of domestic gas boilers with variable natural gas composition”, *Applied Thermal Engineering* **149**, pp. 1052-1060 (2019). DOI: 10.1016/j.applthermaleng.2018.12.106

[10] National Institute of Standards and Technology (NIST). “Atomic Spectra Database, NIST Standard Reference Database 78” (version 5.11). https://www.nist.gov/pml/atomic-spectra-database

[11] I.E. Gordon, L.S. Rothman, R.J. Hargreaves, R. Hashemi, E.V. Karlovets, F.M. Skinner, et al. “The HITRAN2020 molecular spectroscopic database”, *J. Quant. Spectrosc. Radiat. Transfer* **277**, 107949 (2022). https://hitran.org/hitemp/

[12] J. Luque, D.R. Crosley. “LIFBASE: Database and Spectral Simulation Program”. SRI International Report MP 99. https://www.sri.com/platform/lifbase-spectroscopy-tool/

[13] Northern Gas Networks, “Hydrogen Home: About the project”. https://www.northerngasnetworks.co.uk/wp-content/uploads/2022/02/Hydrogen-Home-Information-Leaflet.pdf

[14] A.J. Gee, Y. Yilong, K.K. Foo, A. Chinnici, N. Smith, P.R Medwell. “Toluene addition to turbulent H_2 / natural gas flames in bluff-body burners”, *International Journal of Hydrogen Energy* **47** 27733-27746 (2022). DOI: 10.1016/j.ijhydene.2022.06.154

[15] Y. Yin, P.R Medwell, A.J. Gee, K.K. Foo, B.B. Dally. “Fundamental insights into the effect of blending hydrogen flames with sooting biofuels”, *Fuel* **331**, 125618 (2023). DOI: 10.1016/j.fuel.2022.125618

[16] Department for Business, Energy & Industrial Strategy. “*Hy4Heat. Work Package 2 – Colourant Report*”. https://www.hy4heat.info/s/WP2-Colourant-Report-final-10-May-2021.pdf

[17] Z. Tang, Z. Wang, K. Zhao. “Flame stabilization characteristics of turbulent hydrogen jet flame diluted by nitrogen”, *Energy* **283**, 129100. DOI: 10.1016/j.energy.2023.129100

[18] E.M. Bulewicz, C.G. James, T.M. Sugden. “Photometric investigations of alkali metals in hydrogen flame gases II. The study of excess concentrations of hydrogen atoms in burnt gas mixtures”, *Proceedings of the Royal Society of London. Series A, Mathematical and Physical Sciences*, **235**, pp. 89-106 (1956).

[19] C.G. James, T.M. Sugden. “Photometric investigations of alkali metals in hydrogen flame gases III. The source of the alkali metal continuum”, *Proceedings of the Royal Society of London. Series A, Mathematical and Physical Sciences*, **248**, pp. 238-247 (1958).

[20] P.J. Padley, T.M. Sugden. 1958. “Photometric investigations of alkali metals in hydrogen flame gases IV. Thermal and chemiluminescent effects produced by free radicals.” *Proceedings of the Royal Society of London. Series A, Mathematical and Physical Sciences*, **248**, pp. 248-265 (1958).

[21] https://hydrogen-central.com/northern-gas-networks-hydrogen-homes-open-public/

[22] P.J. Padley. “The origin of the blue continuum in the hydrogen flame”, *The Faraday Society and Contributors*, **56**, pp. 449-454 (1960). DOI: 10.1039/TF9605600449

[23] G. Liu, Y. Wu. “Lift-off height model of hydrogen autoignited flame in turbulent hot air coflow”, *International Journal of Hydrogen Energy*, **49**, pp. 401-412 (2024). DOI: 10.1016/j.ijhydene.2023.08.099

[24] R.R. Chaudhari, R.P. Sahu, S. Ghosh, A. Mukhopadhyay, S. Sen. “Flame color as a lean blowout predictor”, *International Journal of Spray Combustion Dynamics* **5**, 49-65 (2013). DOI: 10.1260/1756-8315.5.1.49

[25] A.R. Choudhuri, S.R. Gollahalli. “Combustion characteristics of hydrogen-hydrocarbon hybrid fuels”, *International Journal of Hydrogen Energy* **25**, pp. 451-462 (2000). DOI: 10.1016/S0360-3199(99)00027-0

[26] M. Najarnikoo, M.Z. Targhi, H. Pasdarshahri. “Experimental study on the flame stability and color characterization of cylindrical premixed perforated burner of condensing boiler by image processing method” *Energy* **189**, 116130. DOI: 10.1016/j.energy.2019.116130

[27] S.H. Won, B. Windom, B. Jiang, Y. Ju. “The role of low temperature fuel chemistry on turbulent flame propagation”, *Combustion and Flame* **161**, 475-483 (2014). DOI: 10.1016/j.combustflame.2013.08.027

[28] E.S. Cho, S.H. Chung. “Improvement of flame stability and NOx reduction in hydrogen-added ultra lean premixed combustion”, *Journal of Mechanics Science and Technology* **23**, pp. 650-658 (2009). DOI: 10.1007/s12206-008-1223-x

[29] M. İlbas, İ. Yılmaz, Y. Kaplan. “Investigations of hydrogen and hydrogen–hydrocarbon composite fuel combustion and NOx emission characteristics in a model combustor”, *International Journal of Hydrogen Energy* **30**, pp. 1139-1147 (2005). DOI: 10.1016/j.ijhydene.2004.10.016

[30] E. Lewis, S.E. Schwartz. “Sea Salt Aerosol Production: Mechanisms, Methods, Measurements and Models”, *Geophysical Monograph 152, American Geophysical Union*, 2004. DOI: 10.1029/GM152

[31] I.S. Cole, W.Y. Chan, G.S. Trinidad, D.A. Paterson. “Holistic model for atmospheric corrosion Part 4 – Geographic information system for predicting airborne salinity”, *Corrosion Engineering, Science and Technology* **39**, pp. 89-96 (2004). DOI: 10.1179/147842204225016831

[32] A. Ooki, M. Uematsu, K. Miura, S. Nakae. “Sources of sodium in atmospheric fine particles”, *Atmospheric Environment* **36**, pp. 4367-4374. DOI: 10.1016/S1352-2310(02)00341-2

[33] S.L. Gong, L.A. Barrie, J.-P. Blanchet. “Modeling sea-salt aerosols in the atmosphere 1. Model development”, *Journal of Geophysical Research* **102**, pp. 3805-3818 (1997). DOI: 10.1029/96JD02953

[34] S.L. Gong, L.A. Barrie, J.M. Prospero, D.L. Savoie, G.P. Ayers, J.-P. Blanchet, L. Spacek. “Modeling sea-salt aerosols in the atmosphere 2. Atmospheric concentrations and fluxes”, *Journal of Geophysical Research* **102**, pp. 3819-3830 (1997). DOI: 10.1029/96JD03401

[35] I.S. Cole, W.D. Ganther, D.A. Paterson, G.A. King, S.A. Furman, D. Lau. “Holistic model for atmospheric corrosion Part 2 – Experimental measurement of deposition of marine salts in a number of long-range studies”, *Corrosion Engineering, Science and Technology* **48**, pp. 259-266 (2004). DOI: 10.1179/147842203225008886

[36] S. Musazzi, U. Perini. “Laser-induced breakdown spectroscopy”, Springer Series in Optical Sciences **182** (2014). DOI: 10.1007/978-3-642-45085-3

[37] J.C. Chow. “Measurement methods to determine compliance with ambient air quality standards for suspended particles”, *Journal of the Air & Waste Management Association* **45**, pp. 320-382 (1995). DOI: 10.1080/10473289.1995.10467369

[38] J.W. Robinson. “Atomic absorption spectroscopy”, *Analytical Chemistry* **32**, pp.17A-29A (1960). DOI: 10.1021/ac60164a712

[39] F.J. Santos, M.T. Galceran, M.T. “The application of gas chromatography to environmental analysis”, *Trends in Analytical Chemistry* **21**, pp.672-685 (2002). DOI: 10.1016/S0165-9936(02)00813-0

[40] P.R. Medwell, Q.N. Chan, B.B. Dally, S. Mahmoud, Z.T. Alwahabi, G.J. Nathan. “Temperature measurements in turbulent non-premixed flames by two-line atomic fluorescence”, *Proceedings of the Combustion Institute* **34**, pp. 3619-3627 (2013). DOI: 10.1016/j.proci.2012.06.027

[41] I.S. Cole, D.A. Paterson, W.D. Ganther. “Holistic model for atmospheric corrosion Part 1 – Theoretical framework for production, transportation and deposition of marine salts”, *Corrosion Engineering, Science and Technology* **38**, pp. 129-134 (2003). DOI: 10.1179/147842203767789203

[42] International Telecommunication Union (ITU), “Studio encoding parameters of digital television for standard 4:3 and wide-screen 16:9 aspect ratios”, Recommendation for television broadcasting service, BT.601-7 (2011). https://www.itu.int/dms_pubrec/itu-r/rec/bt/R-REC-BT.601-7-201103-I!!PDF-E.pdf

Future Fuels CRC

Enabling the Decarbonisation of Australia's Energy Networks

www.futurefuelscrc.com

info@futurefuelscrc.com

Australian Government
Department of Industry, Science and Resources

Cooperative Research Centres Program